Ore Geology Reviews 91 (2017) 432–443

Contents lists available at ScienceDirect

Ore Geology Reviews

journal homepage: www.elsevier.com/locate/oregeorev

In situ Pb and bulk Sr isotope analysis of the Yinchanggou Pb-Zn deposit in Sichuan Province (SW China): Constraints on the origin and evolution of hydrothermal fluids

Shu-Cheng Tan[a], Jia-Xi Zhou[a,b,d,*], Bo Li[c], Jian-Xin Zhao[d]

[a] School of Resource Environment and Earth Science, Yunnan University, Kunming 650500, China
[b] State Key Laboratory of Ore Deposit Geochemistry, Institute of Geochemistry, Chinese Academy of Sciences, Guiyang 550081, China
[c] Faculty of Land Resource Engineering, Kunming University of Science and Technology, Kunming 650093, China
[d] Radiogenic Isotope Facility, School of Earth and Environment Sciences, The University of Queensland, Brisbane, QLD 4072, Australia

ARTICLE INFO

Keywords:
In situ Pb isotopes
Sr isotopes
Origin of mineralizing metals and associated fluids
Evolution of hydrothermal fluids
Carbonate-hosted Pb-Zn deposits
SW China

ABSTRACT

The Yinchanggou Pb-Zn deposit, located in southwestern Sichuan Province, western Yangtze Block, is stratigraphically controlled by late Ediacaran Dengying Formation and contains > 0.3 Mt of metal reserves with 11 wt % Pb + Zn. A principal feature is that this deposit is structurally controlled by normal faults, whereas other typical deposits nearby (e.g. Maozu) are controlled by reverse faults. The origin of the Yinchanggou deposit is still controversial. Ore genetic models, based on conventional whole-rock isotope tracers, favor either sedimentary basin brine, magmatic water or metamorphic fluid sources. Here we use in situ Pb and bulk Sr isotope features of sulfide minerals to constrain the origin and evolution of hydrothermal fluids. The Pb isotope compositions of galena determined by femtosecond LA-MC-ICPMS are as follows: $^{206}Pb/^{204}Pb$ = 18.17–18.24, $^{207}Pb/^{204}Pb$ = 15.69–15.71, $^{208}Pb/^{204}Pb$ = 38.51–38.63. These in situ Pb isotope data overlap with bulk-chemistry Pb isotope compositions of sulfide minerals ($^{206}Pb/^{204}Pb$ = 18.11–18.40, $^{207}Pb/^{204}Pb$ = 15.66–15.76, $^{208}Pb/^{204}Pb$ = 38.25–38.88), and both sets of data plotting above the Pb evolution curve of average upper continental crust. Such Pb isotope signatures suggest an upper crustal source of Pb. In addition, the coarse-grained galena in massive ore collected from the deep part has higher $^{206}Pb/^{204}Pb$ ratios (18.18–18.24) than the fine-grained galena in stockwork ore sampled from the shallow part ($^{206}Pb/^{204}Pb$ = 18.17–18.19), whereas the latter has higher $^{208}Pb/^{204}Pb$ ratios (38.59–38.63) than the former ($^{208}Pb/^{204}Pb$ = 38.51–38.59). However, both types of galena have the same $^{207}Pb/^{204}Pb$ ratios (15.69–15.71). This implies two independent Pb sources, and the metal Pb derived from the basement metamorphic rocks was dominant during the early phase of ore formation in the deep part, whereas the ore-hosting sedimentary rocks supplied the majority of metal Pb at the late phase in the shallow part. In addition, sphalerite separated from different levels has initial $^{87}Sr/^{86}Sr$ ratios ranging from 0.7101 to 0.7130, which are higher than the ore formation age-corrected $^{87}Sr/^{86}Sr$ ratios of country sedimentary rocks ($^{87}Sr/^{86}Sr_{200\ Ma}$ = 0.7083–0.7096), but are significantly lower than those of the ore formation age-corrected basement rocks ($^{87}Sr/^{86}Sr_{200\ Ma}$ = 0.7243–0.7288). Again, such Sr isotope signatures suggest that the above two Pb sources were involved in ore formation. Hence, the gradually mixing process of mineralizing elements and associated fluids plays a key role in the precipitation of sulfide minerals at the Yinchanggou ore district. Integrating all the evidence, we interpret the Yinchanggou deposit as a strata-bound, normal fault-controlled epigenetic deposit that formed during the late Indosinian. We also propose that the massive ore is formed earlier than the stockwork ore, and the temporal-spatial variations of Pb and Sr isotopes suggest a certain potential of ore prospecting in the deep mining area.

1. Introduction

Hydrothermal ore deposits hosted by sedimentary rocks supply the majority of the world's Pb and Zn, as well as a significant proportion of Cu. Generally speaking, sediment-hosted Pb-Zn deposits that contain Pb and/or Zn (rather than e.g. Cu) as their primary commodity have no

* Corresponding author at: State Key Laboratory of Ore Deposit Geochemistry, Institute of Geochemistry, Chinese Academy of Sciences, Guiyang 550081, China.
E-mail address: zhoujiaxi@vip.gyig.ac.cn (J.-X. Zhou).

http://dx.doi.org/10.1016/j.oregeorev.2017.09.012
Received 25 May 2017; Received in revised form 28 July 2017; Accepted 12 September 2017
Available online 14 September 2017
0169-1368/

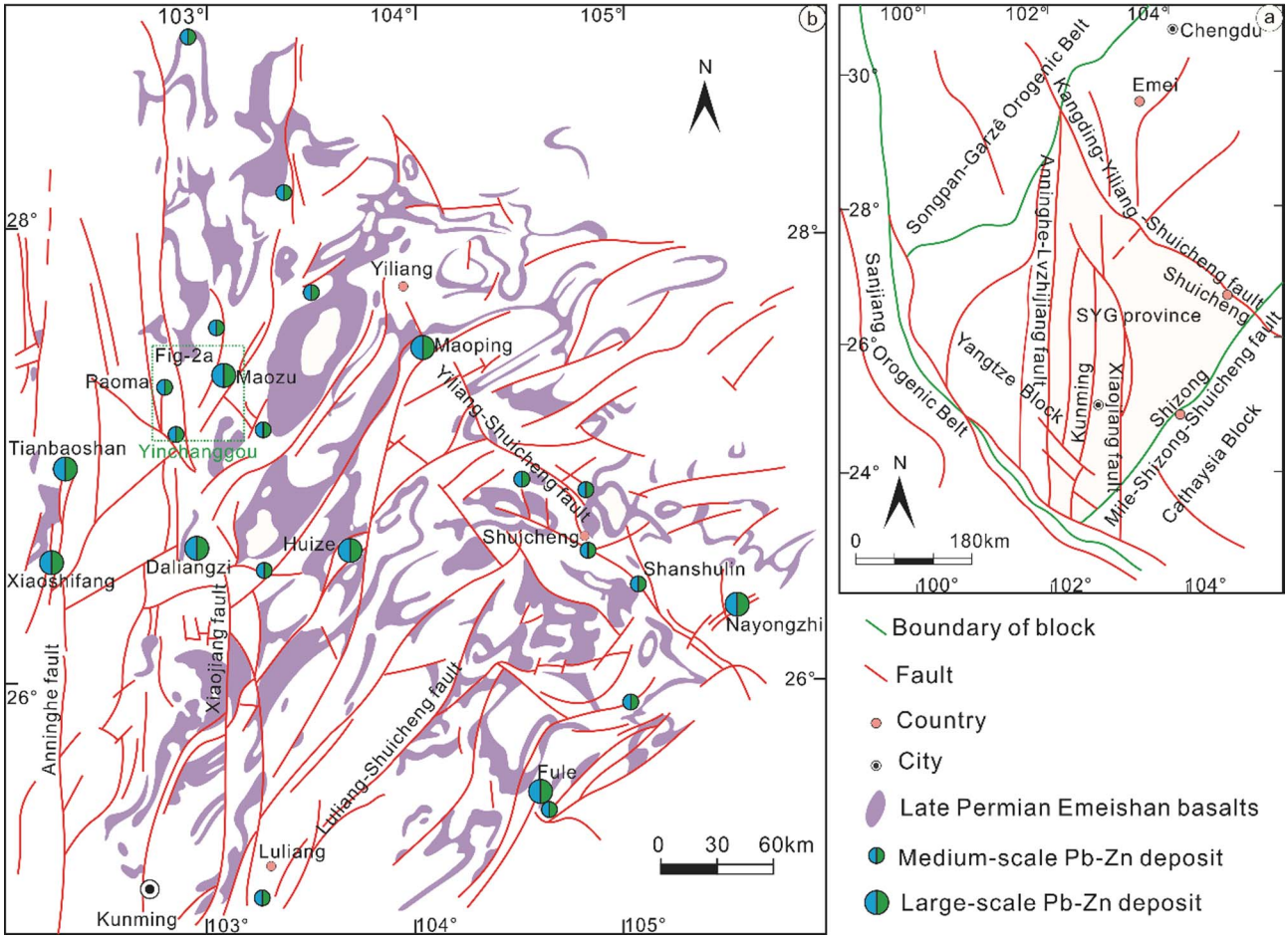

Fig. 1. a: Regional geological setting of Southwest China, highlighting the general study area (modified from Huang et al., 2004); b: Geological sketch map of the Sichuan-Yunnan-Guizhou (SYG) Pb-Zn metallogenic province (modified from Liu and Lin, 1999), which shows the distribution of Pb-Zn ore deposits, Emeishan basalts and faults.

obvious temporal and spatial association with igneous activities (Leach et al., 2005). Such a type of Pb-Zn deposits represents the world's most important source of Pb and Zn, and widely occurs around the world (Heijlen et al., 2003; Leach et al., 2010; Wang et al., 2014). Carbonate-hosted Pb-Zn deposits, a key subtype of sediment-hosted hydrothermal sulfide deposits, are strictly hosted in carbonate platforms (Leach et al., 2005; Wilkinson et al., 2005). The best known carbonate-hosted Pb-Zn deposits occur in the central and western region in the United States, Pine Point in Canada, Upper Silesia in Poland, and Sichuan, Yunnan and Guizhou (SYG) triangular area in China (Heijlen et al., 2003; Leach et al., 2005; Zaw et al., 2007; Zhou et al., 2013a). For example, more than 400 Pb-Zn deposits have been found in the western Yangtze Block (Fig. 1a and b), which form the SYG Pb-Zn metallogenic province (Zhou et al., 2014a). Such a province is an important part of the giant South China low-temperature metallogenic domain (Zhou et al., 2014b; Hu et al., 2017), accounting for 27% of total Zn + Pb resources in China (Zhang et al., 2015). Although extensive research on these Pb-Zn deposits has contributed greatly to our understanding of the metallogeny, the sources of mineralizing elements and associated fluids remain controversial (Zheng and Wang, 1991; Zhou et al., 2001; Xu et al., 2014; Zhou et al., 2014b; Wei et al., 2015; Zhu et al., 2017).

The Yinchanggou deposit, a medium-scale (> 0.3 Mt metal reserves with 11 wt% Pb + Zn) carbonate-hosted Pb-Zn deposit, is located in the central part of the SYG Pb-Zn metallogenic province (Fig. 1b). Unlike other well-studied reverse fault-controlled Pb-Zn deposits (e.g. Maozu, Maoping, Huize and Tianqiao) in the SYG province (Huang et al., 2010; Bai et al., 2013; Zhou et al., 2013a; Wei et al., 2015), this deposit is structurally controlled by normal faults (Figs. 2 and 3). Therefore, the Yinchanggou deposit provides a good opportunity to deepen the understanding of the Pb-Zn mineralization in the SYG province. Although a lot of studies have been carried out on this deposit (Yang, 2009; Zhou, 2009; Yan et al., 2010; Li, 2011; Li et al., 2016), its origin is currently subject to some debates. For example, some studies interpreted it as a distal hydrothermal deposit associated with magmatic water (Yang, 2009; Li, 2011), whereas other investigations considered it to be an example of Mississippi Valley-type (MVT) mineralization (Lin et al., 2010; Wang et al., 2010). In addition, more recent literatures proposed an epigenetic SYG-type model, whereby mineralizing elements and associated fluids were considered to be derived from a mixed source of Emeishan continental flood basalts, ore-hosting marine sedimentary rocks and basement metamorphic rocks (Zhou et al., 2013a; Li et al., 2016).

Radiogenic isotopes are a powerful tool for tracing the origin of mineralizing elements and associated fluids, among which, Pb and Sr isotopes have been widely used for determining the source and evolution of hydrothermal fluids (Carr et al., 1995; Zhou et al., 2001; Wilkinson et al., 2005; Zhou et al., 2016; Li et al., 2015). Microbeam analytical techniques have the potential to provide crucial microscale chemical and isotopic information to reveal the ore formation process and depositional environment of hydrothermal systems (Ikehata et al., 2008; Barker et al., 2009; Ye et al., 2011; Yuan et al., 2015; Jin et al., 2016; Deng et al., 2017). Such information is essential for understanding the genesis of hydrothermal ore deposits. Laser-ablation multi-collector inductively coupled plasma mass spectrometry (LA-MC-ICPMS) is a technique that can efficiently determine in situ isotope compositions of sulfide minerals in hydrothermal systems (Woodhead

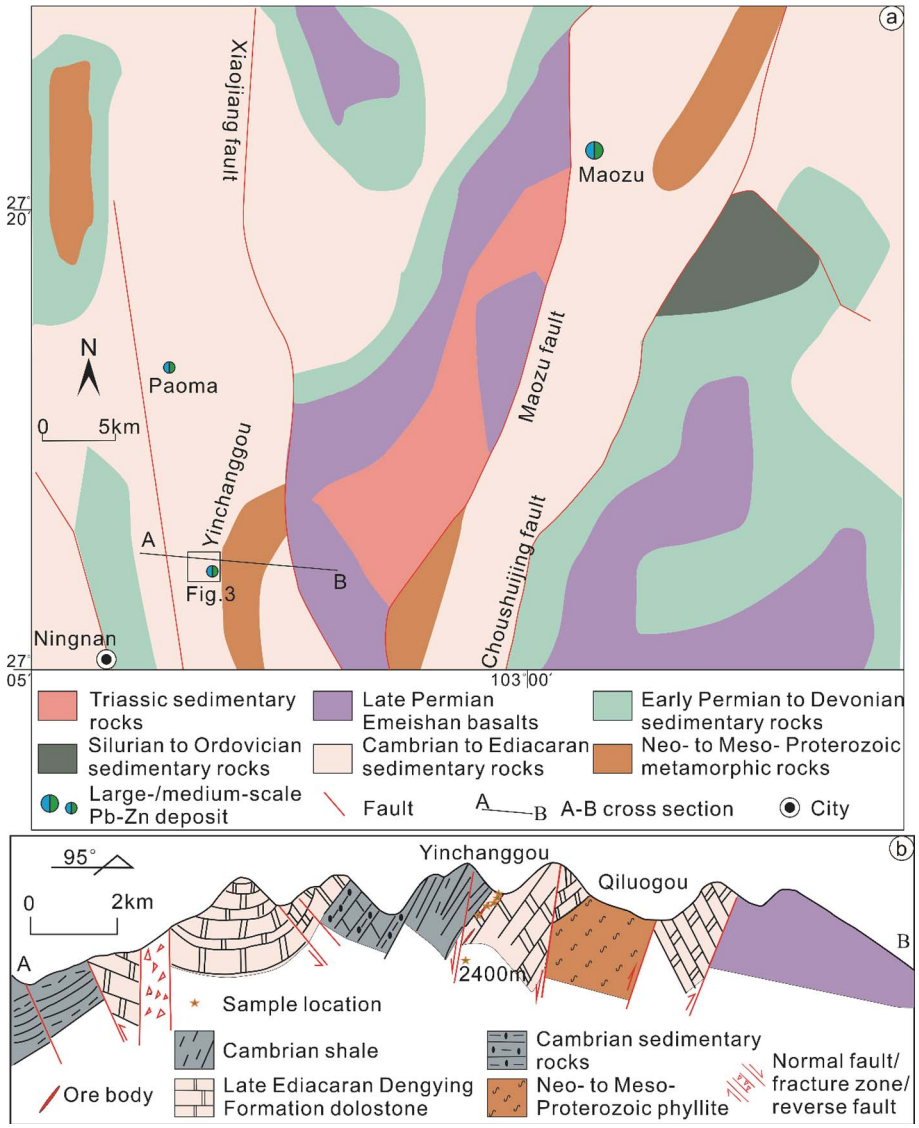

Fig. 2. a: Geological sketch map of the studied region (modified from Li, 2011), which shows the distribution of Pb-Zn deposits, strata and faults; b: A-B cross-section map that presents the strata, faults, folds, ore bodies and lithology (modified from Li et al., 2016).

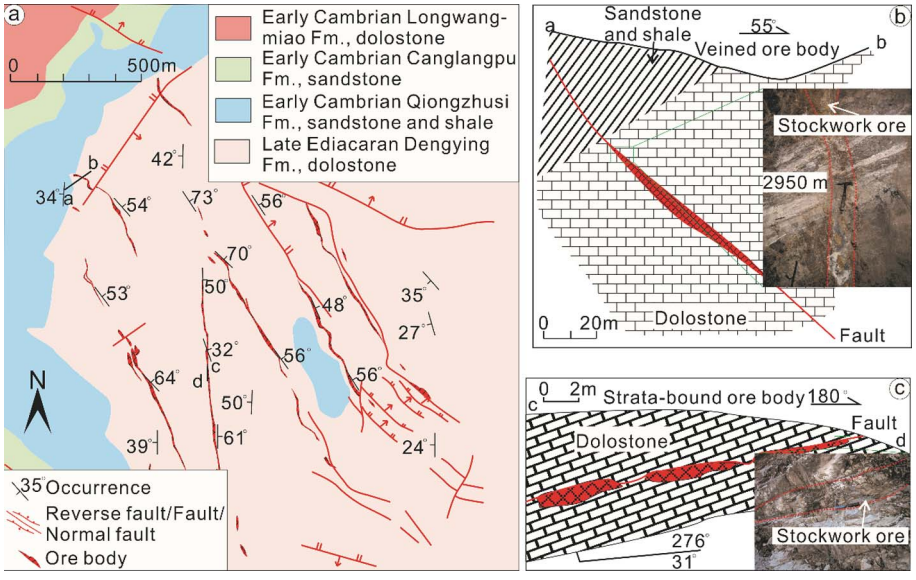

Fig. 3. a: Geological map of the Yinchanggou deposit (modified from Li et al., 2016), which shows the distribution of Pb-Zn ore bodies, strata and faults; b-c: a-b and c-d cross-section maps that present the strata, faults, ore bodies and lithology.

et al., 2009; Chen et al., 2014; Bao et al., 2016).

This paper reports the femtosecond (fs) LA-MC-ICPMS in situ Pb isotope data of galena and Sr isotope data of sphalerite selected from different locations and types of sulfide ores. Through integrating the newly obtained data with conventional whole-rock isotope data and detailed ore deposit geology, this study aims to reveal the origin and evolution of hydrothermal fluids, and to formulate a working metallogenic model for the Yinchanggou deposit. The outcomes are crucial for understanding the ore formation and prospecting in the SYG province, SW China.

2. Geological setting and ore deposit geology

2.1. Geological setting

The studied deposit is situated at the western margin of the Yangtze Block, South China (Fig. 1a). The Yangtze Block is bounded by the Songpan-Ganzê Orogenic Belt to the northwest, the Cathysia Block to the southeast and the Sanjiang Orogenic Belt to the southwest (Fig. 1a). The basement in the western Yangtze Block is late Paleo-Proterozoic to Neo-Proterozoic low-grade metamorphic rocks, which were later intruded by Neo-Proterozoic igneous rocks (Liu and Lin, 1999; Hu et al., 2017). The late Ediacaran to Triassic marine and Jurassic to Cenozoic continental sedimentary rocks composed the sedimentary sequence in the western Yangtze Block (Liu and Lin, 1999; Zhou et al., 2014a). Faults in this region, such as the Xiaojiang fault (Fig. 1b), undergone Hercynian, Indosinian, Yanshanian and Himalayan multi-stage activities, which strictly controlled sedimentation, magmatism and mineralization (Huang et al., 2004; Zhou et al., 2015).

A marked feature in the western Yangtze Block is the ca. 260 Ma Emeishan large igneous province and its flood basalts that cover an area of more than 250,000 km^2 (Zhou et al., 2002; Jian et al., 2009). Another significant feature in the western Yangtze Block is the SYG Pb-Zn metallogenic province and its 408 Pb-Zn deposits that cover an area of more than 170,000 km^2 (Liu and Lin, 1999; Zhou et al., 2014b). These deposits host in late Ediacaran to middle Permian carbonate rocks and have a spatial association with the late Permian Emeishan basalts (Fig. 1b).

After the eruption of the Emeishan basalts, the western Yangtze Block collided with the adjacent blocks, for example Yidun arc, causing the closure of the Paleo-Tethys Ocean (Reid et al., 2007; Hu and Zhou, 2012; Zhou et al., 2013b; Qiu et al., 2016). This event is known as Indosinian Orogeny (257–205 Ma) (e.g. Ren, 1984; Carter et al., 2001) that resulted in the faulting and folding, which significantly controlled the distribution of Pb-Zn deposits in the western Yangtze Block (Liu and Lin, 1999; Zaw et al., 2007; Wang et al., 2014; Zhou et al., 2013a; Zhang et al., 2015). Rb-Sr and Sm-Nd isotope geochronology studies indicate that the ore formation ages of several typical carbonate-hosted Pb-Zn deposits (e.g. Huize, Maozu, Jinshachang, Tianqiao and Paoma) in the SYG province centered around 230–200 Ma (Li et al., 2007; Mao et al., 2012; Zhou et al., 2013a,b, 2015; Zhang et al., 2015). This suggests that the Pb-Zn mineralization in the western Yangtze Block occurred during the late Indosinian, probably in response to the closure of the Paleo-Tethys Ocean.

2.2. Geology of the Yinchanggou ore deposit

Geology of the Yinchanggou ore deposit has been described in detail by Li et al. (2016), therefore only a brief account of the local geology is given here. In the studied region, the exposed strata are of Proterozoic and Paleozoic ages (Fig. 2a; Li, 2011; Li et al., 2016). The Meso- to Neo-Proterozoic Huili Group consists of low-grade metamorphic rocks, such as sandstone and phyllite. These rocks are unconformably overlain by carbonate rocks and black shales of late Ediacaran to Cambrian. A few exposed Ordovician to Silurian sedimentary rocks are unconformably overlain by sandstone and carbonate rocks of Devonian to early Permian ages. All the Devonian to early Permian sedimentary rocks are overlain by late Permian Emeishan flood basalts, in turn, the basalts are overlain by Triassic sedimentary rocks. Tectonic deformation of these rocks formed the Qiluogou anticline (Fig. 2b), which controlled several carbonate-hosted Pb-Zn deposits, such as Paoma and Yinchanggou (Fig. 2a) in the studied region.

In the Yinchanggou ore district, the exposed strata are of late Ediacaran and early Cambrian ages (Fig. 3a). The late Ediacaran Dengying Formation is composed of dolostone. Overlying the dolostone of the Dengying Formation are shale, sandstone and limestone of the early Cambrian Qiongzhusi, Canglangpu and Longwangmiao Formations. Among these rocks, the dolostone and siliceous dolostone of the Dengying Formation are the ore-hosting rocks (Fig. 3a and c).

Tectonics in the Yinchanggou ore district can be divided into NNW-, NNE- and NS-trending groups (Fig. 3a), of which the NNW-trending faults dip NE45° to NE75°, the NNE-trending faults dip SE50° to SE65°, and the NS-trending faults for part of the regional Xiaojiang fault (Fig. 1b). Almost all the fractures in the Yinchanggou ore district are normal faults (Fig. 3a; Li et al., 2016), which have a close association with Pb-Zn ore bodies (Fig. 3a).

Seventeen ore bodies have been found in the Yinchanggou deposit (Fig. 3a; Li et al., 2016). These ore bodies occur either as veins (Fig. 3b) or tabular forms (Fig. 3c), and are structurally controlled by the NS- and NNW-trending normal faults (Fig. 3a and c) and present in the western limb of the Qiluogou anticline (Fig. 2b; Li et al., 2016). Such an ore-controlling style of normal fault-fold tectonic system is significantly distinct from the nearby Maozu deposit that was controlled by reverse fault-fold tectonic system (Figs. 1b, 2a; Zhou et al., 2013b).

In the northern part of the Yinchanggou ore district, ore bodies are NNW-trending with dipping angles of NE45° to NE70° (Fig. 3a and b), whereas ore bodies in the south part trend NS or NNW with dipping angles of NE40° to NE70° (Fig. 3a, c). The majority of ore bodies are 20 m–100 m long and 20 m–80 m wide, with a mean thickness of 3.2 m. All the ore bodies contain a combined metal reserve of more than 0.3 Mt with 0.47 wt% to 12.6 wt% Pb (mean 7.89 wt%), 0.13 wt% to 6.14 wt% Zn (mean 3.27 wt%) and 18.1 to 45.4 g/t Ag (Li, 2011; Li et al., 2016).

Both sulfide and supergene ores are developed in the Yinchanggou ore district. Sulfide ores consists mainly of galena, sphalerite, pyrite, quartz, dolomite and calcite (Fig. 4a–i). Supergene ores are composed dominantly of cerusite, smithsonite, limonite, carbonate minerals and quartz. Ore minerals occur as massive (Fig. 4a–d), veined or stockwork (Fig. 4e-i) structures with euhedral, subhedral, or anhedral coarse- to fine-granular textures (Fig. 4j–i). Galena always shows “pressure shadow” texture (Fig. 4k).

The Yinchanggou deposit has experienced hydrothermal and supergene processes (Li et al., 2016). Two types of sulfide ores formed during the hydrothermal period, namely massive ore (Fig. 4a–d) that consists of euhedral to subhedral coarse-grained sulfide minerals aggregates (pyrite, sphalerite and galena mainly; Fig. 4k–l) and stockwork ore (Fig. 4e–i) that is composed of subhedral to anhedral fine-grained sulfide minerals aggregates (dominantly galena; Fig. 4j). Spatially, the massive ore is commonly found at the bottom part of a single ore body (Li et al., 2016) and occurs mainly in the deep part, whereas the stockwork ore is usually above the massive ore or along the ore-controlling structure, being dominant in the shallow part (Fig. 3c; Zhou, 2009; Li, 2011; Li et al., 2016). In the two types of sulfide ores, gangue quartz and carbonate minerals occur as fragments or fine-veined aggregate cements that fill in the fractures within sulfide aggregation or wall rocks (Fig. 4a–i).

Wall rock alteration in the Yinchanggou ore deposit is characterized by silicification or Fe-Mn/Ca-Mg carbonatization (Fig. 3b and c), both of which can be divided into pre- and post-ore two subtypes. The pre-ore silicification formed siliceous dolostone that hosts ore bodies, whereas the post-ore quartz occurred as siliceous bands or cements in wall rocks (Fig. 4a–i). Dolomitic limestone or coarse-grained re-

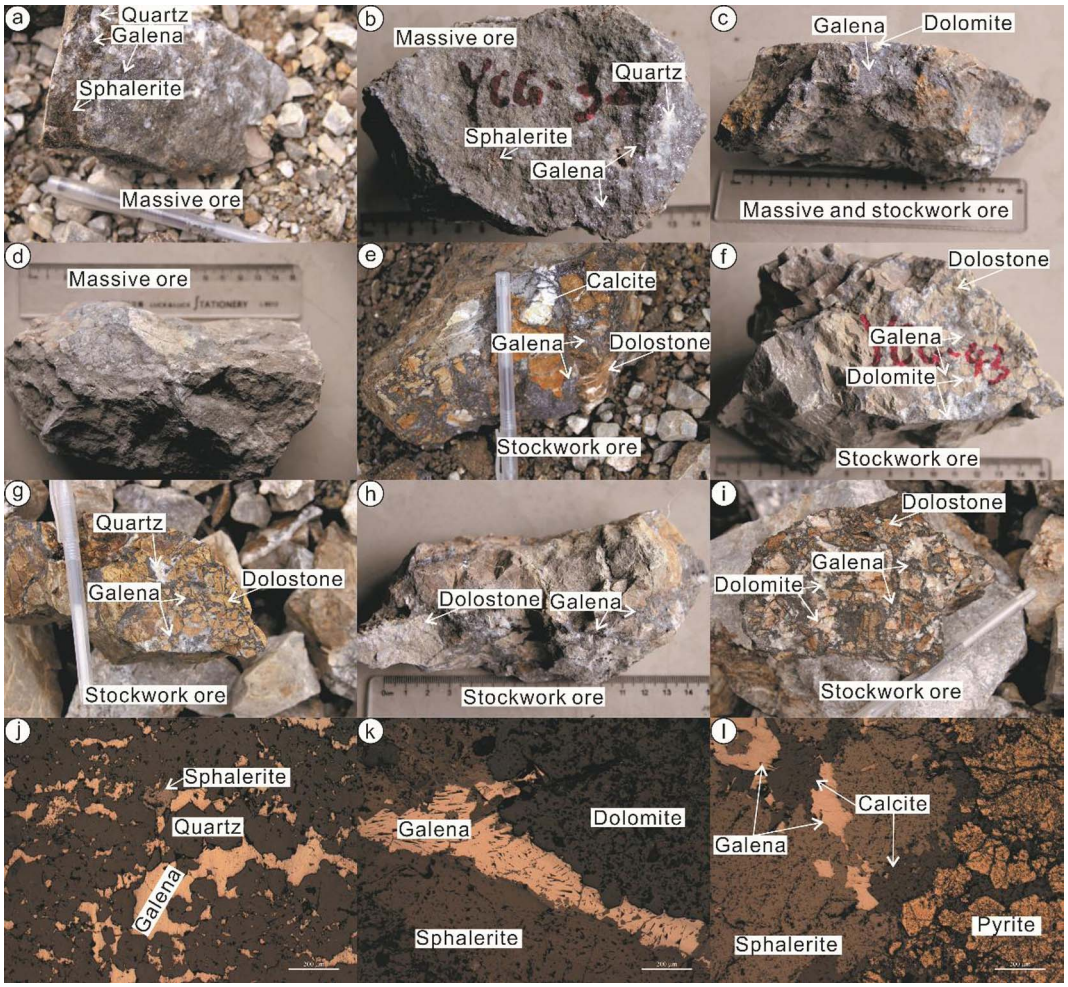

Fig. 4. Main features and textures of sulfide ores in the Yinchanggou deposit. a-b: Massive ore, quartz occurs as cement within dense sulfide aggregate; c: Massive ore, dolomite presents as spotted cement within dense sulfide aggregate; d: Massive ore, dense sulfide aggregate; e: Stockwork ore, galena occurs as fine-vein and cements brecciated dolostone, calcite occurs as fragments; f: Stockwork ore, galena and dolomite present as fine-vein and cement brecciated dolostone; g: Stockwork ore, quartz and galena present as fine-veined aggregate and cement brecciated dolostone; h: Stockwork ore, galena presents as fine-vein and cements brecciated dolostone; i: Stockwork ore, galena and dolomite occur as fine-vein and cements brecciated dolostone; j: Late phase fine-grained sphalerite coexists with late phase fine-veined galena, and all of them are enclosed by late phase quartz; K: Early phase coarse-grained sphalerite coexists with early coarse-grained galena and dolomite; l: Early phase pyrite occurs as euhedral to subhedral coarse-grain and coexists with early phase xenomorphic coarse-grained sphalerite and galena, while calcite cements the sulfide minerals.

crystallized dolostone formed during the pre-ore carbonatization process. The post-ore veinlets or stockworks of calcite/dolomite aggregates fill in the fractures within wall rocks (Figs. 3b and c, 4a–i). The net veined calcite/dolomite can be used as a key indicator for ore prospecting.

3. Samples and analytical methods

3.1. Samples

Samples were collected from drill holes and underground mining tunnels. Forty polished thin sections of sulfide ores were used for mineralogical observation, and then six polished thin sections (massive and stockwork ores) and five massive ore samples were selected for in situ Pb isotope analysis and sphalerite microdrill separation. The location of studied samples was marked on Fig. 2b. Sphalerite separates were used for Rb-Sr isotope analysis. In situ Pb isotope ratios of sphalerite and pyrite were not determined, due to the high Hg contents in them that could dramatically affect the quality of the data (Chen et al., 2014).

3.2. Analytical methods

3.2.1. In situ Pb isotope analysis

In situ Pb isotope analysis was completed at the State Key Laboratory of Continental Dynamics, Northwest University, using a Nu II MC-ICPMS (Nu Instruments, Wrexham, UK) combined with a 266 nm NWR UP Femto femtosecond (fs) laser ablation system (ESI, USA). The surface of polished thin section was cleaned using Milli-Q (18.2 MΩ cm) water before analysis. Line scan ablation consisted of background collection for 20 s followed by 50 s of laser ablation for signal collection. Laser ablation parameters are listed as follows: spot size, 15 μm; 100% output energy, > 600 μJ; 100% energy density, 6 J/cm^2; laser frequency, 5–50 Hz; and ablation way, line 3 μm/s. This ensures a strong enough Pb signal for the analysis of galena. The Tl (20×10^{-9}, NIST SRM 997, $^{205}Tl/^{203}Tl = 2.38890$) and NIST SRM 610 glass were served as internal and external standards, respectively. The repeated analysis of NIST SRM 610 glass standard yielded highly reliable and reproducible results during the whole analytical process with mean $^{206}Pb/^{204}Pb = 17.052 \pm 0.003$, $^{207}Pb/^{204}Pb = 15.515 \pm 0.003$ and $^{208}Pb/^{204}Pb = 36.980 \pm 0.007$ (1s, $n = 183$). The details of fs LA-MC-ICPMS in situ Pb isotope analysis and instrument parameters are available in Yuan et al. (2015) and Bao et al. (2016).

Table 1
In situ Pb isotope ratios of galena in massive and brecciated ores from the Yinchanggou deposit.

No.	Mineral	$^{206}Pb/^{204}Pb$	1 s	$^{207}Pb/^{204}Pb$	1 s	$^{208}Pb/^{204}Pb$	1 s	$^{208}Pb/^{206}Pb$	1 s	$^{207}Pb/^{206}Pb$	1 s
YCG-32-01	2400 m; Coarse-grained galena in massive ore	18.244	0.003	15.704	0.003	38.570	0.007	2.1142	0.0001	0.86079	0.00003
YCG-32-02		18.224	0.002	15.704	0.002	38.558	0.006	2.1158	0.0001	0.86173	0.00003
YCG-32-03		18.237	0.003	15.704	0.003	38.569	0.007	2.1149	0.0001	0.86114	0.00003
YCG-32-04		18.208	0.002	15.697	0.002	38.534	0.006	2.1162	0.0001	0.86209	0.00002
YCG-32-05		18.206	0.003	15.699	0.003	38.536	0.007	2.1167	0.0001	0.86231	0.00003
YCG-32-06		18.239	0.003	15.708	0.003	38.575	0.009	2.1151	0.0001	0.86130	0.00003
YCG-32-07		18.240	0.003	15.710	0.003	38.586	0.008	2.1154	0.0001	0.86131	0.00003
YCG-32-08		18.233	0.003	15.698	0.003	38.549	0.007	2.1143	0.0001	0.86101	0.00003
YCG-41-01		18.236	0.003	15.704	0.003	38.564	0.008	2.1148	0.0001	0.86115	0.00003
YCG-41-02		18.230	0.003	15.702	0.003	38.558	0.008	2.1151	0.0001	0.86137	0.00003
YCG-41-03		18.213	0.002	15.693	0.003	38.526	0.007	2.1155	0.0001	0.86170	0.00003
YCG-41-04		18.206	0.002	15.696	0.002	38.531	0.006	2.1164	0.0001	0.86215	0.00003
YCG-41-05		18.218	0.002	15.703	0.003	38.558	0.007	2.1166	0.0001	0.86204	0.00003
YCG-41-06		18.224	0.003	15.705	0.003	38.564	0.009	2.1162	0.0001	0.86186	0.00004
YCG-41-07		18.223	0.003	15.703	0.003	38.558	0.007	2.1160	0.0001	0.86175	0.00003
YCG-42-01		18.185	0.002	15.695	0.002	38.519	0.006	2.1182	0.0001	0.86314	0.00002
YCG-42-02		18.186	0.003	15.698	0.003	38.525	0.008	2.1184	0.0001	0.86320	0.00003
YCG-42-03		18.181	0.002	15.693	0.002	38.511	0.007	2.1184	0.0001	0.86324	0.00003
YCG-42-04		18.179	0.002	15.694	0.003	38.513	0.007	2.1185	0.0001	0.86329	0.00003
YCG-42-05		18.181	0.003	15.696	0.003	38.520	0.007	2.1188	0.0001	0.86341	0.00003
YCG-43-01	2950 m; Fine-grained galena in stockwork ore	18.175	0.002	15.700	0.002	38.611	0.006	2.1244	0.0001	0.86380	0.00002
YCG-43-02		18.173	0.003	15.699	0.003	38.605	0.007	2.1243	0.0001	0.86389	0.00003
YCG-43-03		18.182	0.002	15.704	0.003	38.622	0.007	2.1242	0.0001	0.86375	0.00003
YCG-43-04		18.173	0.002	15.693	0.002	38.590	0.006	2.1234	0.0001	0.86352	0.00002
YCG-43-05		18.184	0.003	15.705	0.003	38.622	0.008	2.1240	0.0001	0.86365	0.00003
YCG-43-06		18.182	0.002	15.701	0.003	38.613	0.007	2.1237	0.0001	0.86356	0.00003
YCG-43-07		18.190	0.003	15.707	0.003	38.630	0.007	2.1237	0.0001	0.86351	0.00003
YCG-47-01		18.184	0.003	15.700	0.003	38.611	0.008	2.1234	0.0001	0.86344	0.00003
YCG-47-02		18.185	0.003	15.701	0.003	38.612	0.007	2.1233	0.0001	0.86341	0.00003
YCG-47-03		18.172	0.002	15.698	0.002	38.608	0.006	2.1246	0.0001	0.86388	0.00003
YCG-47-04		18.176	0.003	15.698	0.003	38.603	0.007	2.1240	0.0001	0.86368	0.00003
YCG-47-05		18.175	0.003	15.699	0.003	38.606	0.008	2.1241	0.0001	0.86373	0.00003
YCG-47-06		18.173	0.003	15.698	0.003	38.606	0.009	2.1243	0.0001	0.86375	0.00003
YCG-51-01		18.182	0.003	15.702	0.003	38.615	0.008	2.1237	0.0001	0.86357	0.00003
YCG-51-02		18.180	0.003	15.703	0.003	38.615	0.007	2.1242	0.0001	0.86372	0.00003
YCG-51-03		18.183	0.002	15.703	0.002	38.618	0.007	2.1238	0.0001	0.86358	0.00003
YCG-51-04		18.181	0.002	15.697	0.003	38.598	0.007	2.1231	0.0001	0.86334	0.00003
YCG-51-05		18.188	0.002	15.700	0.002	38.612	0.006	2.1230	0.0001	0.86321	0.00003
YCG-51-06		18.192	0.003	15.702	0.003	38.621	0.008	2.1230	0.0001	0.86314	0.00003
YCG-51-07		18.192	0.003	15.699	0.003	38.614	0.008	2.1226	0.0001	0.86298	0.00003

3.2.2. Bulk Sr isotope analysis

Chemical separation of Rb and Sr from matrix elements and mass spectrometric measurements were accomplished at the Beijing Research Institute of Uranium Geology. Spec-Sr ion exchange resin was used for the separation and purification of Rb and Sr. The procedure blanks of Rb and Sr are about 6 and 5 pg (10^{-12} g), respectively. A detailed analytical procedure for Rb-Sr isotope analysis is available in Li et al. (2005) and is similar to literatures (Zhou et al., 2013a, 2014b). Rb-Sr isotope ratios were measured by the GV Isoprobe-T thermal ionization mass spectrometer (TIMS). An $^{88}Sr/^{86}Sr$ ratio of 8.37521 is used to calibrate mass fractionation of Sr isotopes. The mean $^{87}Sr/^{86}Sr$ ratio of NBS 987 standard is 0.710243 ± 6 (2σ, n = 10). The uncertainties (2σ) are 0.005% for $^{87}Sr/^{86}Sr$ ratios and 2% for $^{87}Rb/^{86}Sr$ ratios (Li et al., 2005).

4. Analytical results

4.1. In situ Pb isotope ratios

In situ Pb isotope ratios of galena are presented in Table 1 and are shown in Figs. 5–7. Galena has in situ Pb isotope ratios as follows: $^{206}Pb/^{204}Pb$ = 18.17–18.24, $^{207}Pb/^{204}Pb$ = 15.69–15.71, $^{208}Pb/^{204}Pb$ = 38.51–38.63. All the in situ Pb isotope data overlap with the previous Pb isotope data of sulfide minerals through bulk-chemistry ($^{206}Pb/^{204}Pb$ = 18.11–18.40, $^{207}Pb/^{204}Pb$ = 15.66–15.76, $^{208}Pb/^{204}Pb$ = 38.25–38.88; Table 2; Fig. 5a; Li, 2011; Li et al., 2016). A principal feature is that galena in massive ore collected at 2400 m altitude has higher $^{206}Pb/^{204}Pb$ ratios (18.18–18.24) than galena in stockwork ore sampled at 2950 m altitude ($^{206}Pb/^{204}Pb$ = 18.17–18.19), whereas the latter has higher $^{208}Pb/^{204}Pb$ ratios (38.59–38.63) than the former ($^{208}Pb/^{204}Pb$ = 38.51–38.59), but both of them have the same $^{207}Pb/^{204}Pb$ ratios (15.69–15.71). Furthermore, these in situ Pb isotope data show significant grouping in Pb-Pb diagrams (Figs. 6 and 7). On the other hand, although the location and type of previous samples are not clear, the bulk Pb isotope data also can be divided into two groups that are similar to those of in situ Pb isotope data (Figs. 5b and c, 7a).

4.2. Bulk Rb-Sr isotope ratios

The Rb-Sr isotope data of sphalerites are listed in Table 3 and are shown in Fig. 8. Sphalerite samples have very low contents of Rb (0.014–0.058 × 10^{-6}) and relatively low Sr concentrations (3.83–13.5 × 10^{-6}). The $^{87}Rb/^{86}Sr$ ratios of the five sphalerite samples range from 0.0061 to 0.0395 and the $^{87}Sr/^{86}Sr$ ratios range from 0.71015 to 0.71311. The $^{87}Sr/^{86}Sr$ ratios of sphalerite separates from the Yinchanggou deposit are lower than those of the nearby Paoma and Maozu deposits (Table 3; Fig. 8a). In addition, sphalerite collected from the deep part (2750 m) of the Yinchanggou ore district contains higher $^{87}Sr/^{86}Sr$ ratios (0.7131) than those sampled from the shallow part ($^{87}Sr/^{86}Sr$ = 0.7102–0.7114, 2907–2960 m) (Fig. 8b).

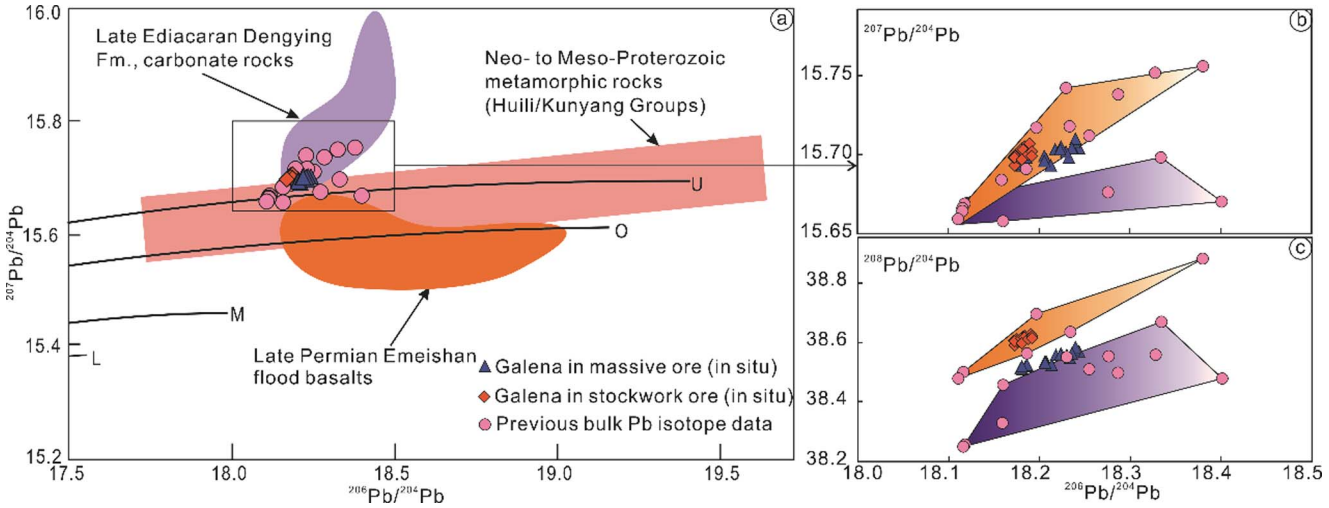

Fig. 5. a: Plot of $^{207}Pb/^{204}Pb$ vs. $^{206}Pb/^{204}Pb$ that presents the comparison between galena and the U, O, M and L Pb evolution lines (Zartman and Doe, 1981), as well as ore formation age-corrected (200 Ma) Emeishan basalts, ore-hosting sedimentary rocks and basement metamorphic rocks (Liu and Lin, 1999; Huang et al., 2004; Li et al., 2007; Zhou et al., 2013a, 2014a); Upper Crust (U), Orogen Belt (O), Mantle (M) and Lower Crust (L); Plots of $^{207}Pb/^{204}Pb$ vs. $^{206}Pb/^{204}Pb$ (b) and $^{208}Pb/^{204}Pb$ vs. $^{206}Pb/^{204}Pb$ (c) that presents the comparison between in situ and bulk Pb isotope data.

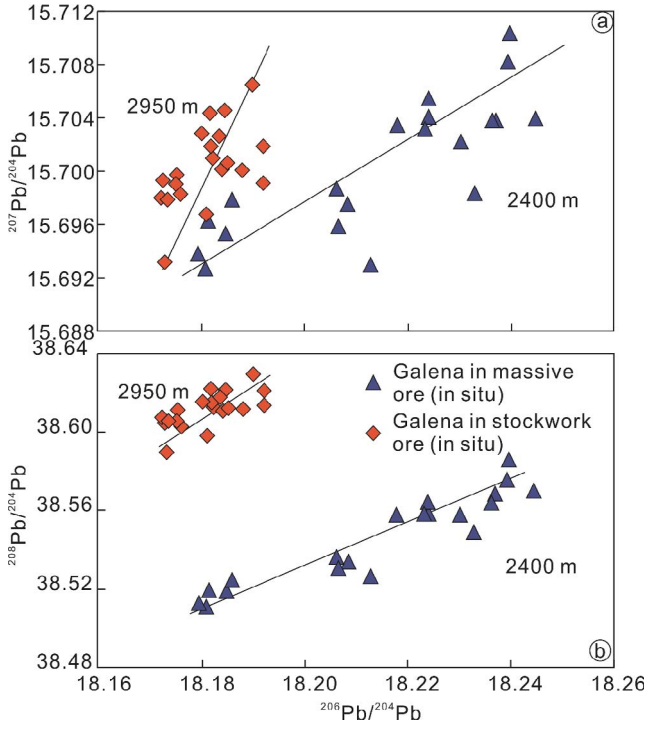

Fig. 6. Plots of in situ $^{207}Pb/^{204}Pb$ vs. $^{206}Pb/^{204}Pb$ (a) and $^{208}Pb/^{204}Pb$ vs. $^{206}Pb/^{204}Pb$ (b) that present the Pb evolution curves of galena in massive ore at 2400 m and stockwork ore at 2950 m altitudes.

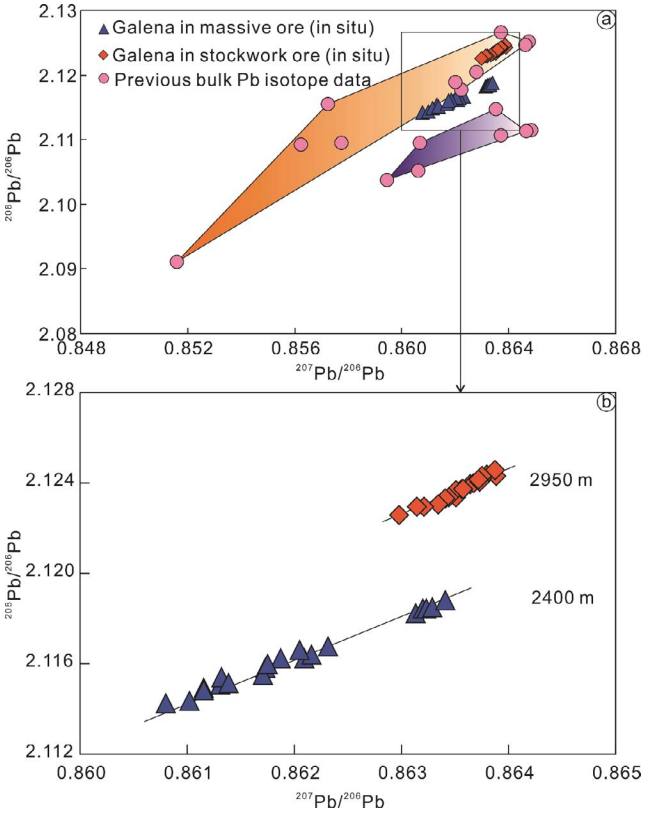

Fig. 7. a: Plot of $^{207}Pb/^{206}Pb$ vs. $^{208}Pb/^{206}Pb$ that presents the comparison between in situ and bulk Pb isotope data; b: Plot of in situ $^{207}Pb/^{206}Pb$ vs. $^{208}Pb/^{206}Pb$ that presents the Pb evolution curves of galena in massive ore at 2400 m and stockwork ore at 2950 m altitudes.

5. Discussion

5.1. Origin of mineralizing elements and associated fluids

5.1.1. New constraints from in situ Pb isotope compositions

U and Th contents in galena are extremely low, therefore, the time-integrated effect of their radiogenic decays on radiogenic Pb isotopes is negligible (Carr et al., 1995; Muchez et al., 2005; Pass et al., 2014; Zhou et al., 2016). Therefore, the obtained Pb isotope ratios of galena can approximate to that of hydrothermal fluids. In the plot of $^{207}Pb/^{204}Pb$ vs. $^{206}Pb/^{204}Pb$ (Fig. 5a), both the bulk and in situ Pb isotope data of galena plot above the Pb evolution curve of average upper continental crust, indicating a clear upper crustal source of Pb (Zartman and Doe, 1981).

Based on previous extensive research on the carbonate-hosted Pb-Zn deposits in the SYG province, three potential Pb sources have been proposed, i.e. the spatially associated Emeishan basalts, ore-hosting sedimentary rocks and basement metamorphic rocks (Huang et al., 2004; Zhou et al., 2013a, 2014b; Li et al., 2015, 2016). Compared with the ore formation age-corrected (200 Ma; Mao et al., 2012; Zhou et al.,

Table 2
Previous bulk Pb isotope ratios of sulfide minerals from the Yinchanggou deposit.

No.	Object	$^{206}Pb/^{204}Pb$	$^{207}Pb/^{204}Pb$	$^{208}Pb/^{204}Pb$	$^{208}Pb/^{206}Pb$	$^{207}Pb/^{204}Pb$	Sources
YO-4	Galena	18.276	15.676	38.553	2.1095	0.8577	Li et al., 2016
YO-9	Galena	18.160	15.658	38.458	2.1177	0.8622	
YO-12	Galena	18.334	15.698	38.670	2.1092	0.8562	
YO-17	Galena	18.118	15.669	38.256	2.1115	0.8648	
YO-29	Galena	18.116	15.666	38.500	2.1252	0.8648	
QO-7	Galena	18.116	15.664	38.249	2.1113	0.8647	
QO-9	Galena	18.230	15.742	38.551	2.1147	0.8635	
QO-22	Galena	18.380	15.756	38.884	2.1156	0.8572	
QO-25	Galena	18.401	15.670	38.479	2.0911	0.8516	
Y05	Galena	18.186	15.691	38.564	2.1205	0.8628	
Y11	Sphalerite	18.328	15.752	38.558	2.1038	0.8595	
Y20	Sphalerite	18.287	15.738	38.498	2.1052	0.8606	
RQD002-1	Sphalerite	18.255	15.712	38.510	2.1096	0.8607	Li, 2011
RQLG29-1	Sphalerite	18.159	15.684	38.328	2.1107	0.8637	
YMT14-2	Sphalerite	18.234	15.718	38.637	2.1190	0.8620	
14RKPT6-1	Sphalerite	18.111	15.659	38.479	2.1246	0.8646	
RQLG32-1	Sphalerite	18.197	15.717	38.698	2.1266	0.8637	

2013a,b, 2015; Zhang et al., 2015) whole-rock Pb isotope ratios of the basalts (Fig. 5a), sulfide minerals from the Yinchanggou deposit display higher $^{207}Pb/^{204}Pb$ ratios than the basalts at given $^{206}Pb/^{204}Pb$ ratios. This rules out a single source of Pb that was derived mainly from the basalts. Furthermore, all the Pb isotope data fall into the overlapping field of the sedimentary rocks and metamorphic rocks (Fig. 5a), suggesting a probable mixed Pb source of host and basement rocks.

In the plots of $^{207}Pb/^{204}Pb$ vs. $^{206}Pb/^{204}Pb$ (Fig. 5b) and $^{208}Pb/^{204}Pb$ vs. $^{206}Pb/^{204}Pb$ (Fig. 5c), both the in situ and bulk Pb isotope data define two separate trends. Further, in the in situ $^{207}Pb/^{204}Pb$ vs. $^{206}Pb/^{204}Pb$ (Fig. 6a) and $^{208}Pb/^{204}Pb$ vs. $^{206}Pb/^{204}Pb$ plots (Fig. 6b), such two separate evolution trends for the galena in massive and stockwork ores are much clearer. As the pressure shadow is the most common texture in galena (Fig. 4k), the impurities within the galena crystals could significantly affect the quality of the obtained bulk-chemistry Pb isotope data (Bao et al., 2016; Jin et al., 2016). Hence, we suggest that in situ Pb isotope signatures could better reflect the nature of ore-forming fluids. On the other hand, as the range of $^{206}Pb/^{204}Pb$ and $^{208}Pb/^{204}Pb$ ratios for the two types of galena (0.07 for galena in massive ore and 0.12 for galena in stockwork ore; Table 1) is significantly higher than the analytical uncertainly of in situ Pb isotope data (1s, 0.003 and 0.008, respectively), such two distinct curves should have geological implications. This means that there are two independent Pb sources. Moreover, in the $^{208}Pb/^{206}Pb$ vs. $^{207}Pb/^{206}Pb$ plot (Fig. 7a), both the in situ and bulk Pb isotope data also show two trends. Furthermore, in the in situ $^{208}Pb/^{206}Pb$ vs. $^{207}Pb/^{206}Pb$ plot (Fig. 7b), the Pb isotope evolution curves for the two types of galena have remarkable difference. Again, this suggests that the metal Pb sources for the two types of galena are clearly distinct and the homogenization of associated fluids had not occurred before the precipitation of sulfide minerals. On the other hand, the evidence of ore deposit geology (Figs. 2 and 3) and mineralogy (Fig. 4) implies that massive ore formed earlier than stockwork ore.

Integrating all the above evidence, we propose that although both ore-hosting sedimentary rocks and basement metamorphic rocks supply the metal Pb for the formation of the Yinchanggou deposit, the basement-derived Pb was dominant during the early phase in the deep part, whereas the host rocks supplied the majority of metal Pb at the late phase in the shallow part. This is supported by geological records (Fig. 2a; exposed Neo- to Meso-Proterozoic metamorphic rocks) and H—O isotope data (early phase fluids was dominated by metamorphic fluids) (Li et al., 2016), as well as Sr isotope signatures (see below).

Table 3
Sr isotope ratios of sphalerite from the Yinchanggou, and the nearby Paoma and Maozu deposits.

No.	Location	Mineral	$Rb/10^{-6}$	$Sr/10^{-6}$	$^{87}Rb/^{86}Sr$	$^{87}Sr/^{86}Sr$	2σ	$^{87}Sr/^{86}Sr_{\ 200\ Ma}$	Sources
YO-4	2750 m	Sphalerite	0.050	3.83	0.0378	0.71311	0.00001	0.71300	This paper
YO-23	2907 m	Sphalerite	0.058	4.23	0.0395	0.71140	0.00002	0.71129	
YO-24	2935 m	Sphalerite	0.014	4.47	0.0089	0.71110	0.00001	0.71107	
YO-26	2960 m	Sphalerite	0.017	4.68	0.0104	0.71125	0.00002	0.71122	
YO-29	2950 m	Sphalerite	0.028	13.5	0.0061	0.71015	0.00001	0.71013	
PM-1	Paoma	Sphalerite	0.326	1.95	0.4837	0.71592	0.00004	0.71454	Lin et al., 2010
PM-2		Sphalerite	0.431	3.15	0.3948	0.71594	0.00006	0.71481	
PM-3		Sphalerite	0.166	2.18	0.2199	0.71545	0.00003	0.71482	
PM-4		Sphalerite	0.039	6.70	0.0167	0.71487	0.00003	0.71482	
PM-5		Sphalerite	0.128	0.848	0.4367	0.71607	0.00001	0.71482	
PM-6		Sphalerite	0.556	2.99	0.5361	0.71592	0.00005	0.71439	
PM-7		Sphalerite	0.085	0.855	0.2864	0.71537	0.00007	0.71455	
PM-8		Sphalerite	0.255	11.0	0.0670	0.71521	0.00001	0.71500	
PM-9		Sphalerite	0.148	5.05	0.0847	0.71506	0.00002	0.71482	
PM-10	Maozu	Sphalerite	0.087	4.98	0.0503	0.71529	0.00003	0.71515	
MZ-5		Sphalerite	0.050	0.330	0.4704	0.718700	0.000017	0.71745	Zheng et al., 2015
MZ-18		Sphalerite	0.060	2.86	0.0588	0.710785	0.000013	0.71061	
MZ-21		Sphalerite	0.100	0.360	0.8497	0.720965	0.000012	0.71868	
MZ-34		Sphalerite	0.060	0.920	0.1834	0.716921	0.000010	0.71638	
MZ-37		Sphalerite	0.180	10.02	0.0519	0.711738	0.000014	0.71159	

$(^{87}Sr/^{86}Sr)_t = {}^{87}Sr/^{86}Sr - {}^{87}Sr/^{87}Rb\ (e^{\lambda t} - 1)$, $\lambda_{Rb} = 1.41 \times 10^{-11}\ t^{-1}$, $t = 200$ Ma.

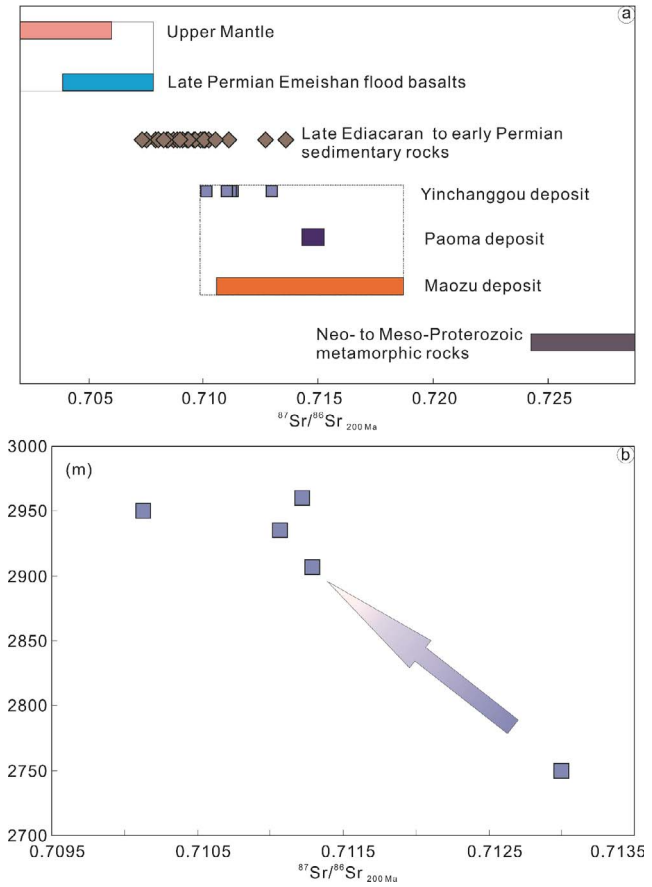

Fig. 8. a: Comparison of initial $^{87}Sr/^{86}Sr$ ratios between sphalerite and Upper Mantle, Emeishan basalts, early Permian to late Ediacaran sedimentary rocks and Neo- to Meso-Proterozoic metamorphic rocks (Li and Qin, 1988; Chen and Ran, 1992; Deng et al., 2000; Shi et al., 2003; Huang et al., 2004; Jiang and Li, 2005; Zhou et al., 2013a, 2014b); b: The variation of initial $^{87}Sr/^{86}Sr$ ratios of sphalerite in massive ore sampled from 2750 m to 2960 m altitudes.

5.1.2. Evidence from Rb-Sr isotope compositions

Although the real status of Rb and Sr isotopes in sphalerite is unclear, direct Rb-Sr dating of sphalerite is still commonly used by far (Nakai et al., 1990; Brannon et al., 1992; Christensen et al., 1995; Li et al., 2005; Zhou et al., 2013a). Sphalerite Rb-Sr isochron dating is very difficult and is not always successful, just as a case in this study (Table 3), whereas the Sr isotopes have been widely used to constrain the origin and evolution of hydrothermal fluids (Ni et al., 2012; Zhou et al., 2013a; Deng et al., 2015). However, as was demonstrated by previous studies, minor impurities like clays will change the Sr isotope compositions of sphalerite obviously (Nakai et al., 1990; Christensen et al., 1995), so the purity of sphalerite is the key to ensure reliable Sr isotope data. In fact, sphalerite used in this study was obtained by micro-drilling technology (see above section 3.1), which could reduce the influence of impurities to the greatest extent.

In order to use Sr isotopes of hydrothermal minerals to trace the source of mineralizing elements and associated fluids, we need to know the initial $^{87}Sr/^{86}Sr$ ratio (Deng et al., 2000; Gromek et al., 2012; Ni et al., 2012). Geochronological studies indicate that the ore formation ages of the Pb-Zn deposits in the SYG province are between 230 Ma and 200 Ma, peaking at 200 Ma (Mao et al., 2012; Zhou et al., 2013a, 2015; Zhang et al., 2015). Thus an ore formation age of 200 Ma was used to calculate the initial $^{87}Sr/^{86}Sr$ ratios of sphalerite from the Yinchanggou deposit and all the potential metal source rocks (i.e. basalts, sedimentary rocks and metamorphic rocks) in the SYG province (e.g. Huang et al., 2004; Zhou et al., 2014b). The $^{87}Sr/^{86}Sr_{200\ Ma}$ ratios of basalts (and upper mantle: 0.704 ± 0.002; Faure, 1977) range from 0.7039 to 0.7078 (average 0.7058; Table 4; Fig. 8a; Huang et al., 2004), which are significantly lower than those of sphalerite (0.7101–0.7130, mean 0.7113). In contrast, the $^{87}Sr/^{86}Sr_{200\ Ma}$ ratios of metamorphic rocks range from 0.7243 to 0.7288 (average 0.7268; Table 4; Fig. 8a; Li and Qin, 1988; Chen and Ran, 1992), which are dramatically higher than those of sphalerite (0.7101–0.7130, mean 0.7113). Neither the basements nor the basalts match the initial Sr isotope ratios of sphalerite (Fig. 8a), suggesting that neither of them involved solely in ore formation. On the other hand, sedimentary rocks have the $^{87}Sr/^{86}Sr_{200\ Ma}$ ratios ranging from 0.7073 to 0.7136 (average 0.7097; Table 4; Fig. 8a; Hu, 1999; Deng et al., 2000; Shi et al., 2003; Jiang and Li, 2005; Zhou et al., 2013a, 2014b), which are similar to those of sphalerite (0.7101–0.7130, mean 0.7113). This suggests that the ore-forming fluids were most likely derived from or flowed through country sedimentary rocks (Table 4; Fig. 8a). However, except for the black shales of early Cambrian, other sedimentary rocks (especially the ore-hosting Dengying Formation dolostone) contain much lower $^{87}Sr/^{86}Sr_{200\ Ma}$

Table 4
Sr isotope ratios of whole-rock of metamorphic rocks, sedimentary rocks, Emeishan flood basalts and Upper Mantle.

Sample No.	Rock	$Rb/10^{-6}$	$Sr/10^{-6}$	$^{87}Rb/^{86}Sr$	$^{87}Sr/^{86}Sr$	$^{87}Sr/^{86}Sr_{200Ma}$	Reference
	Late Permian basalts	0.7039–0.7078 (N = 85, mean 0.7058)					Huang et al., 2004
D11	Early Permian Limestone	0.098	267	0.001	0.7075	0.7075	Zhou et al., 2014b
D12	Early Permian Limestone	0.064	254	0.001	0.7073	0.7073	
LMG-9	Early Permian Limestone	0.087	186	0.001	0.7079	0.7079	Deng et al., 2000
D8	Late Carboniferous Limestone	0.408	162	0.007	0.7100	0.7100	Zhou et al., 2013a
D9	Late Carboniferous Limestone	1.20	169	0.020	0.7100	0.7099	
D35	Early Carboniferous Dolostone	0.244	66	0.010	0.7101	0.7101	Zhou et al., 2014b
D36	Early Carboniferous Dolostone	0.030	81.9	0.001	0.7099	0.7099	
D13	Early Carboniferous Dolostone	0.009	67	0.000	0.7093	0.7093	Hu, 1999
D14	Early Carboniferous Dolostone	0.005	54.0	0.000	0.7087	0.7087	
D15	Early Carboniferous Dolostone	0.500	77.0	0.006	0.7093	0.7093	
D6	Late Devonian Limestone	1.38	76.2	0.0511	0.7085	0.7083	Zhou et al., 2013a
D7	Late Devonian Limestone	0.034	350	0.0003	0.7088	0.7088	
LMG-11	Middle Devonian Dolostone	4.84	99.6	0.1325	0.7105	0.7101	Deng et al., 2000
D3	Middle Devonian Sandstone	15.2	58.2	0.7365	0.7132	0.7111	Zhou et al., 2013a
	Early Cambrian Carbonate rocks	0.7084–0.7099 (N = 16, mean 0.7091)					Shi et al., 2003
	Early Cambrian Black shale	0.7120–0.7136 (N = 2, mean 0.7128)					Jiang and Li, 2005
D1	Late Ediacaran Dolostone	0.204	308	0.0019	0.7083	0.7083	Zhou et al., 2013a
D2	Late Ediacaran Dolostone	2.26	108	0.0590	0.7098	0.7096	
Neo- to Meso-Proterozoic Metamorphic rocks		0.7243–0.7288 (N = 5, mean 0.7266)					Cong, 1988; Li and Qin, 1988; Chen and Ran, 1992
Upper Mantle		0.704 ± 0.002					Faure, 1977

$(^{87}Sr/^{86}Sr)_t = {}^{87}Sr/^{86}Sr - {}^{87}Sr/^{87}Rb\ (e^{\lambda t} - 1)$, $\lambda_{Rb} = 1.41 \times 10^{-11}\ t^{-1}$, t = 200 Ma.

Table 5
A brief comparison of the Yinchanggou and the nearby Paoma and Maozu deposits.

Ore deposit	Yinchanggou	Paoma	Maozu
Ore grade (Pb + Zn)	Massive ore: 14 wt%; Stockwork ore: 3.9–9.6 wt%	6–9 wt%, partly > 30 wt%	11.4 wt%, partly > 15 wt%
Ore tonnage (Pb + Zn)	> 0.3 Mt	> 0.2 Mt	2 Mt
Ore-hosting strata	Late Ediacaran Dengying Formation	Late Ediacaran Dengying Formation	Late Ediacaran Dengying Formation
Ore-hosting lithology	Dolostone	Dolostone	Dolostone
Ore-controlling structure	SN- and NNW-trending normal fault and Qiluogou anticline	SN- and NNW-trending normal fault and Qiluogou anticline	NE-trending Maozu reverse fault and two anticline-syncline fold systems
Late Ediacaran paleogeography	Ningnan-Huidong basin	Ningnan-Huidong basin	Eastern margin of Ningnan-Huidong basin
Ore formation age	Late Triassic	Sphalerite Rb-Sr age: 200.1 ± 4.0 Ma	Calcite Sm-Nd age: 196 ± 13 Ma
Mineral assemblage	Galena, sphalerite, pyrite, dolomite and calcite	Galena, sphalerite, pyrite, dolomite, quartz, calcite, fluorite and barite	Sphalerite, galena, pyrite, dolomite, calcite and fluorite
S isotopes	$\delta^{34}S$ = +5.8 to +20.3‰		$\delta^{34}S$ = +8.8 to +19.9‰
Pb isotopes	$^{206}Pb/^{204}Pb$ = 18.11–18.40, $^{207}Pb/^{204}Pb$ = 15.66–15.76, $^{208}Pb/^{204}Pb$ = 38.25–38.88		$^{206}Pb/^{204}Pb$ = 18.13–18.38, $^{207}Pb/^{204}Pb$ = 15.64–15.69, $^{208}Pb/^{204}Pb$ = 38.22–38.58
Sr isotopes	$^{87}Sr/^{86}Sr$ = 0.7102–0.7131	$^{87}Sr/^{86}Sr$ = 0.7149–0.7161	$^{87}Sr/^{86}Sr$ = 0.7108–0.7210
Reference	Li, 2011; Li et al., 2016	Lin et al., 2010	Zhou et al., 2013b; Zheng et al., 2015

ratios (0.7083–0.7096, mean 0.7089; Table 4) than those of sphalerite (0.7101–0.7130, mean 0.7113). In fact, Zhou et al. (2015) reported that early Cambrian black shales not only contain high $^{87}Sr/^{86}Sr$ ratios, but also are rich in radiogenic Pb ($^{206}Pb/^{204}Pb$ = 20.950–22.354, $^{207}Pb/^{204}Pb$ = 15.837–15.930, $^{208}Pb/^{204}Pb$ = 40.878–41.928), which are significantly higher than both in situ and bulk Pb isotope ratios of sulfide minerals (Table 1; Figs. 5 and 7). Also, our Pb isotope data rule out the main contribution of Emeishan basalts (Fig. 5a). In addition, the nearby Paoma and Maozu deposits that have the same source to the Yinchanggou deposit, containing much higher initial $^{87}Sr/^{86}Sr$ ratios than those of country sedimentary rocks (Fig. 8a). Therefore, we propose that Sr isotope features support the involvement of the basement and host rocks in mineralization (Fig. 8a). On the other hand, the initial Sr isotope ratio (0.7130) of sphalerite sampled from the deep part (2750 m) is higher than those collected from the shallow part (0.7101–0.7113, 2907–2960 m; Fig. 8b), indicating that the basement rocks play a much more significant role in the deep part of the Yinchanggou ore district than the shallow part, as suggested by in situ Pb isotopes (see above; Figs. 5–7) and H—O isotopes (metamorphic fluids was dominant in the early phase) (Li et al., 2016).

5.2. Evolution of hydrothermal fluids and ore prospecting

5.2.1. Evolution of hydrothermal fluids

Isotopes can not only trace the source of ore-forming elements and associated fluids, but also reveal the evolution process (Carr et al., 1995; Huang et al., 2004; Zhou et al., 2014a). Our in situ Pb and bulk Sr isotope data show that the samples collected from the deep part of the Yinchanggou ore district contains higher $^{206}Pb/^{204}Pb$ (Fig. 6a) and $^{87}Sr/^{86}Sr$ (Fig. 8b) ratios, but lower $^{208}Pb/^{204}Pb$ (Fig. 6b) and $^{208}Pb/^{206}Pb$ (Fig. 7b) ratios than those sampled from the shallow part. Through comparison of all the potential Pb sources, we find that the source of high $^{206}Pb/^{204}Pb$ and $^{87}Sr/^{86}Sr$ ratios is corresponding to the basement rocks (Figs. 5a, 8a). Moreover, the mineralogy (Fig. 4) indicates that the coarse-grained galena formed earlier than the fine-grained galena. The combined evidence indicates that the early phase hydrothermal fluids was probably dominated by basement-derived metamorphic fluids, whereas the late phase hydrothermal fluids was probably the country rocks-derived basin brine, and thus the evolution tendency of hydrothermal fluids from the deep to shallow parts is reasonable (Figs. 6–8). Such a migration tendency of hydrothermal fluids can be used for ore prospecting (see below).

5.2.2. Ore targeting

Because of the well-developed stockwork ore (Figs. 3–4) in the Yinchanggou deposit, some researches considered that this deposit may do not have ore prospecting potential, which results in their abandonment by mining companies. In this study, we find that the basement-derived Pb is dominated in the massive ore at the early phase, whereas the host rocks-derived Pb is predominated in stockwork ore at the late phase (Figs. 5–7). The former is occurred significantly in the deep part of the Yinchanggou ore district, whereas the latter presents mainly in the shallow part (Fig. 3b and c; Zhou, 2009; Li, 2011; Li et al., 2016). Additionally, the variation in Sr isotopes of sphalerite collected from 2750 m (0.7130) to 2960 m depths (0.7101–0.7113) also indicates the basement with more radiogenic Sr provided the majority of mineralizing elements and associated fluids in the deep part (Fig. 8a and b). Previous studies indicated that the more ore-forming elements were derived from the basements, the more metallogenic potential and the higher ore grade (Huang et al., 2004; Zhou et al., 2013a, 2014a). For example, the Maozu deposit that contains more radiogenic Sr isotopes (Fig. 8a) has more than 2 Mt of metal reserves (Tables 3, 5; Zhou et al., 2013b). On the other hand, the post-ore stockwork calcite and dolomite, an important ore prospecting clue, is also well-developed in the Yinchanggou ore district (Fig. 3b and c). Hence, we propose that basement-derived massive ore may have a certain potential in the deep part and the distribution of the host rocks-derived stockwork ore can be used as a direct clue for ore prospecting.

5.3. Ore formation processes

5.3.1. Timing of mineralization and sulfide precipitation mechanism

The geological records (Figs. 1–4) and isotopic evidence (Figs. 5–8; Li, 2011; Li et al., 2016) indicate the Yinchanggou deposit is an epigenetic deposit, which should form significantly younger than the ore-hosting Ediacaran strata age. In addition, the Yinchanggou deposit is structurally controlled by normal fault-fold tectonic system (Figs. 2b, 3a–c), which was active during the late Indosinian Orogeny (Liu and Lin, 1999; Zhou, 2009). This suggests that the formation of the Yinchanggou deposit was most likely around the late Indosinian. Moreover, in the studied region, there are several typical Pb-Zn deposits hosted in the Dengying Formation, such as Paoma and Maozu (Figs. 1b, 2a), which have sphalerite Rb-Sr isochron age of 200.1 ± 4.0 Ma (Lin et al., 2010) and calcite Sm-Nd isochron age of 196 ± 13 Ma (Zhou et al., 2013b), respectively. A brief comparison of the Yinchanggou, Paoma and Maozu deposits suggests that they are similar in geological setting, mineral and isotope compositions, as well as mineralization (Table 5). The only difference is that the Maozu deposit is structurally controlled by reverse fault and has a large-scale ore tonnage (Table 5). Hence, it is highly likely that the Yinchanggou ore

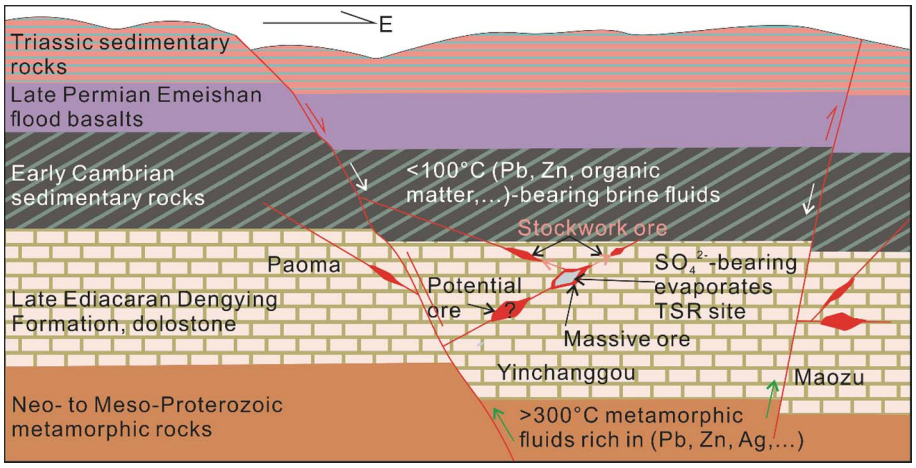

Fig. 9. A working metallogenic model of Pb-Zn mineralization in the studied region.

deposit formed simultaneously to the Paoma and Maozu at late Triassic.

Three genetic models have been employed to explain the precipitation of sulfide minerals in sediment-hosted Pb-Zn deposits: reduced S, local sulfate reduction, or metal and reduced S-mixing (Leach et al., 2005). The reduced S model requires ore-forming metals and reduced S to be transported together to the depositional site; the local sulfate reduction model requires that the concentration of reduced S at the depositional site increases through sulfate reduction; the metal and reduced S-mixing needs the mixing of a metal-rich but reduced S-poor brine with a fluid rich in hydrogen sulfide at the depositional site (Leach et al., 2005). The S isotope data of sulfide minerals ($\delta^{34}S$ = + 5.8 to + 20.3‰) suggest that the source of S is marine sulfate within ore-hosting strata and TSR dominated the formation of S^{2-} from SO_4^{2-} (Li et al., 2016). Our in situ Pb and Sr isotope data indicate that two independent metal sources of basement and host rocks (Figs. 5–8) are reasonable. In addition, the massive ore (dominated by basement-derived metals) was formed earlier than stockwork ore (predominated by host rocks-originated metals) (Figs. 3–4). Therefore, the local sulfate reduction model plays a key role in the formation of massive ore at the early phase, whereas metal and reduced S-mixing model dominates the formation of stockwork ore during the late phase in the Yinchanggou deposit.

5.3.2. Ore genesis model

Integrating all available information, we interpret the Yinchanggou deposit as a strata-bound, normal fault-controlled epigenetic deposit that formed during the late Indosinian. Our working metallogenic model is described as follows: The ca. 260 Ma Emeishan magmatism elevated the background geothermal gradient, which facilitates and enhances the mobilization and extraction of mineralizing elements from the basement metamorphic rocks (Zhou et al., 2013b). Driven by the Indosinian Orogeny (257–205 Ma), the basement-derived metamorphic hydrothermal fluids (rich in Pb, Zn and Ag) migrated upward along the regional faults (such as Xiaojiang, Figs. 1b, 9), and then released into sub-tectonic systems, where they mixed with the (a little Pb, Zn) organic matter-bearing brine fluids, and migrated together to the depositional site that contains SO_4^{2-}-bearing evaporates (Fig. 9); This heated mixture resulted in the formation of S^{2-} from SO_4^{2-} by the process of thermochemical sulfate reduction (TSR), and thus caused massive sulfide precipitation; Then fluid/rock reaction led to host rocks-sourced metal and reduced S-mixing, resulting in the formation of stockwork ore front/upon massive ore along the ore-controlling structures or within the wall rocks (Figs. 9, 3b-c).

6. Conclusions

Based on this study, the following conclusions can be reached: (1) In situ Pb and bulk Sr isotope data imply basement metamorphic rocks provided the majority of metal Pb for the formation of massive ore at the early phase in the deep part, whereas host rocks-derived Pb dominated the formation of stockwork ore during the late phase at the shallow part; (2) The mixing of two fluids and evaporates plays a key role in the formation of the Yinchanggou sulfide ore; (3) The Yinchanggou Pb-Zn deposit is a strata-bound, normal fault-controlled epigenetic deposit and formed at the late Indosinian; and (4) the net veined calcite or dolomite and stockwork ore, together with the temporal and spatial variations of Pb and Sr isotopes imply a certain potential of massive ore prospecting in the deep part.

Acknowledgements

This research was financially supported by the Key Project of National Natural Science Foundation of China (41430315), the National Basic Research Program of China (2014CB440905) and the Visiting Scholar Project of China Scholarship Council to J.-X. Zhou. We thank Prof. Hong-Lin Yuan and Dr. Zhi-An Bao (Northwest University) for kind help with Pb isotope analysis, and Prof. Jian-Guo Gao and Prof. Ying-Shu Li (Kunming University of Science and Technology) for useful discussions. Comments and suggestions from Prof. Franco Pirajno (Editor-in-Chief), Prof. Yan-Jing Chen (Associate Editor) and two anonymous reviewers greatly improved the quality of the paper.

References

Bai, J., Huang, Z., Zhu, D., Yan, Z., Zhou, J., 2013. Isotopic compositions of sulfur in the Jinshachang lead-zinc deposit, Yunnan, China, and its implication on the formation of sulfur-bearing minerals. Acta Geol. Sin. 87, 1355–1369.

Bao, Z., Yuan, W., Yuan, H., Liu, X., Chen, K., Zong, C., 2016. Non-matrix-matched determination of lead isotope ratios in ancient bronze artifacts by femtosecond laser ablation multi-collector inductively coupled plasma mass spectrometry. Int. J. Mass Spectrom. 402, 12–19.

Barker, S.L., Hickey, K.A., Cline, J.S., Dipple, G.M., Kilburn, M.R., Vaughan, J.R., Longo, A.A., 2009. Uncloaking invisible gold: use of nanoSIMS to evaluate gold, trace elements, and sulfur isotopes in pyrite from Carlin-type gold deposits. Econ. Geol. 104, 897–904.

Brannon, J.C., Podosek, F.A., McLimans, R.K., 1992. Alleghenian age of the Upper Mississippi Valley zinc-lead deposit determined by Rb-Sr dating of sphalerite. Nature 356, 509–511.

Carr, G.R., Dean, J.A., Suppel, D.W., Heithersay, P.S., 1995. Precise lead isotope fingerprinting of hydrothermal activity associated with Ordovician to Carboniferous metallogenic events in the Lachlan fold belt of New South Wales. Econ. Geol. 90, 1467–1505.

Carter, A., Roques, D., Bristow, C., Kinny, P., 2001. Understanding Mesozoic accretion in Southeast Asia: significance of Triassic thermotectonism (Indosinian orogeny) in Vietnam. Geology 29, 211–214.

Chen, H.S., Ran, C.Y., 1992. Isotope Geochemistry of Copper Deposit in Kangdian Area. Geological Publishing House, Beijing, pp. 1–25 (in Chinese).

Chen, K.Y., Yuan, H.L., Bao, Z.A., Zong, C.L., Dai, M.N., 2014. Precise and accurate in situ determination of lead isotope ratios in NIST, USGS, MPI-DING and CGSG glass reference materials using femtosecond laser ablation MC-ICP-MS. Geostand. Geoanal. Res. 38, 5–21.

Christensen, J.N., Halliday, A.N., Vearncombe, J.R., Kesler, S.E., 1995. Testing models of

large-scale crustal fluid flow using direct dating of sulfides; Rb-Sr evidence for early dewatering and formation of mississippi valley-type deposits, Canning Basin. Australia. Econ. Geol. 90, 877–884.
Cong, B.L., 1988. Evolution and Formation of Panxi Rift. Science Press, Beijing, pp. 10–33 (in Chinese).
Deng, H.L., Li, C.Y., Tu, G.Z., Zhou, Y.M., Wang, C.W., 2000. Strontium isotope geochemistry of the Lemachang independent silver ore deposit, northeastern Yunnan, China. China Earth Sci. 43, 337–346.
Deng, X.H., Chen, Y.J., Bagas, L., Zhou, H.Y., Yao, J.M., Zheng, Z., Wang, P., 2015. Isotope (S-Sr-Nd-Pb) constraints on the genesis of the ca. 850Ma Tumen Mo-F deposit in the Qinling Orogen, China. Precambr. Res. 266, 108–118.
Deng, J., Wang, C., Bagas, L., Selvaraja, V., Jeon, H., Wu, B., Yang, L., 2017. Insights Into Ore Genesis of the Jinding Zn-Pb Deposit. Evidence from Zn and in-situ S isotopes. Ore Geol. Rev, Yunnan Province, China 10.1016/j.oregeorev.2016.10.036.
Faure, G., 1977. Principles of Isotope Geology. John Wiley & Sons, New York, pp. 28–110.
Gromek, P., Gleeson, S.A., Simonetti, A., 2012. A basement-interacted fluid in the N81 deposit, Pine Point Pb-Zn district, Canada: Sr isotopic analyses of single dolomite crystals. Mineral. Deposita 47, 749–754.
Heijlen, W., Muchez, P., Banks, D.A., Schneider, J., Kucha, H., Keppens, E., 2003. Carbonate-hosted Zn-Pb deposits in Upper Silesia, Poland: origin and evolution of mineralizing fluids and constraints on genetic models. Econ. Geol. 98, 911–932.
Hu, Y.G., 1999. Ag Occurrence, Source of Ore-forming Metals and Mechanism of Yinchangpo Ag-Pb-Zn Deposit, Guizhou (Ph.D. Thesis). Institute of Geochemistry, Chinese Academy of Sciences, pp. 10–55 (in Chinese with English abstract).
Hu, R.Z., Zhou, M.F., 2012. Multiple Mesozoic mineralization events in South China-an introduction to the thematic issue. Mineral. Deposita 47, 579–588.
Hu, R., Fu, S., Huang, Y., Zhou, M., Fu, S., Zhao, C., Wang, Y., Bi, X., Xiao, J., 2017. The giant South China Mesozoic low-temperature metallogenic domain: reviews and a new geodynamic model. J. Asian Earth Sci. 137, 9–34.
Huang, Z.L., Chen, J., Han, R.S., Li, W.B., Liu, C.Q., Zhang, Z.L., Ma, D.Y., Gao, D.R., Yang, H.L., 2004. Geochemistry and Ore-formation of the Huize Giant Lead-zinc Deposit, Yunnan, Province, China-Discussion on the Relationship Between Emeishan flood Basalts and Lead-zinc Mineralization. Geological Publishing House, Beijing, pp. 1–204 (in Chinese).
Huang, Z., Li, X., Zhou, M., Li, W., Jin, Z., 2010. REE and C-O isotopic geochemistry of calcites from the world-class Huize Pb-Zn deposits, Yunnan, China: Implications for the ore genesis. Acta Geol. Sin. 84, 597–613.
Ikehata, K., Notsu, K., Hirata, T., 2008. In situ determination of Cu isotope ratios in copper-rich materials by NIR femtosecond LA-MC-ICP-MS. J. Anal. Atomic Spectrom. 23, 1003–1008.
Jian, P., Li, D.Y., Kröner, A., Zhang, Q., Wang, Y.Z., Sun, X.M., Zhang, W., 2009. Devonian to Permian plate tectonic cycle of the Paleo-Tethys Orogen in southwest China (II): insights from zircon ages of ophiolites, arc/back-arc assemblages and within-plate igneous rocks and generation of the Emeishan CFB province. Lithos 113, 767–784.
Jiang, Y.H., Li, S.R., 2005. Study on the isotope data tracing and isotopic chronology in the black-rock series type Ni-Mo deposit in the Lower Cambrian in Hunan and Guizhou provinces. J. Mineral. Petrol. 25, 62–66 (in Chinese with English abstract).
Jin, Z.G., Zhou, J.X., Huang, Z.L., Ye, L., Luo, K., Gao, J.G., Chen, X.L., Wang, B., Peng, S., 2016. Ore genesis of the Nayongzhi Pb-Zn deposit, Puding city, Guizhou Province, China: evidences from S and in situ Pb isotopes. Acta Petrol. Sin. 32, 3441–3455 (in Chinese with English abstract).
Leach, D.L., Sangster. D., Kelley, K.D., Large, R.R., Garven, G., Allen, C., Gutzmer, J., Walters, S., 2005. Sediment-hosted lead-zinc deposits: A global perspective. Econ. Geol. 100th Ann. Volume, pp. 561–607.
Leach, D.L., Bradley, D.C., Huston, D., Pisarevsky, S.A., Taylor, R.D., Gardoll, S.J., 2010. Sediment-hosted lead-zinc deposits in Earth history. Econ. Geol. 105, 593–625.
Li, W., 2011. The Geochemical Characteristics and the Cause of Ore Deposit Formation in Yinchanggou-Qiluogou Lead-zinc Deposit, Ningnan, Sichuan (Master degree thesis). Chengdu University of Technology (in Chinese with English abstract).
Li, F.H., Qin, J.M., 1988. Presinian System in Kangdian Area. Chongqing Press, Chongqing, pp. 15–45 (in Chinese).
Li, Q.L., Chen, F.K., Wang, X.L., Li, C.F., 2005. Ultra-low procedural blank and the single grain mica Rb-Sr isochron dating. Chin. Sci. Bull. 50, 2861–2865.
Li, W.B., Huang, Z.L., Yin, M.D., 2007. Dating of the giant Huize Zn-Pb ore field of Yunnan province, southwest China: constraints from the Sm-Nd system in hydrothermal calcite. Resour. Geol. 57, 90–97.
Li, B., Zhou, J.X., Huang, Z.L., Yan, Z.F., Bao, G.P., Sun, H.R., 2015. Geological, rare earth elemental and isotopic constraints on the origin of the Banbanqiao Zn-Pb deposit, southwest China. J. Asian Earth Sci. 111, 100–112.
Li, B., Zhou, J., Li, Y., Chen, A., Wang, R., 2016. Geology and isotope geochemistry of the Yinchanggou-Qiluogou Pb-Zn Deposit, Sichuan Province, Southwest China. Acta Geol. Sin. 90, 1768–1779.
Lin, Z.Y., Wang, D.H., Zhang, C.Q., 2010. Rb-Sr isotopic age of sphalerite from the Paoma lead-zinc deposit in Sichuan Province and its implications. Geol. China 37, 196–488 (in Chinese with English abstract).
Liu, H.C., Lin, W.D., 1999. Study on the Law of Pb-Zn-Ag Ore Deposit in Northeast Yunnan, China. Yunnan University Press, Kunming, pp. 1–468 (in Chinese).
Mao, J.W., Zhou, Z.H., Feng, C.Y., Wang, Y.T., Zhang, C.Q., Peng, H.J., Miao, Y., 2012. A preliminary study of the Triassic large-scale mineralization in China and its geodynamic setting. Geol. China 39, 1437–1471 (in Chinese with English abstract).
Muchez, P., Heijlen, W., Banks, D., Blundell, D., Boni, M., Grandia, F., 2005. Extensional tectonics and the timing and formation of basin-hosted deposits in Europe. Ore Geol. Rev. 27, 241–267.
Nakai, S.I., Halliday, A.N., Kesler, S.E., Jones, H.D., 1990. Rb-Sr dating of sphalerites from Tennessee and the genesis of Mississippi Valley type ore-deposits. Nature 346, 354–357.
Ni, Z.Y., Chen, Y.J., Li, N., Zhang, H., 2012. Pb-Sr-Nd isotope constraints on the fluid source of the Dahu Au-Mo deposit in Qinling Orogen, central China, and implication for Triassic tectonic setting. Ore Geol. Rev. 46, 60–67.
Pass, H.E., Cookem, D.R., Davidson, G., Maas, R., Dipple, G., Rees, C., Ferreira, L., Taylor, C., Deyell, C.L., 2014. Isotope geochemistry of the northeast zone, Mount Polley alkalic Cu-Au-Ag porphyry deposit, British Columbia: A case for carbonate assimilation. Econ. Geol. 109, 859–890.
Qiu, L., Tang, S.L., Wang, Q., Yang, W.X., Tang, X.L., Wang, J.B., 2016. Mesozoic geology of southwestern China: Indosinian foreland overthrusting and subsequent deformation. J. Asian Earth Sci. 122, 91–105.
Reid, A., Wilson, C.J.L., Shun, L., Pearson, N., Belousova, E., 2007. Mesozoic plutons of the Yidun Arc, SW China: U-Pb geochronology and Hf isotopic signature. Ore Geol. Rev. 31, 88–106.
Ren, J.S., 1984. The Indosinian orogeny and its significance in the tectonic evolution of China. Acta Geosici. Sin. 6, 31–42.
Shi, H., Huang, S.J., Shen, L.C., Zhang, M., 2003. Strontium isotope composition of the Cambrian Luojiaguo section in Xiushan, Chongqing and its stratigraphic significance. J. Stratigraphy 27, 71–76 (in Chinese with English abstract).
Wang, C., Deng, J., Zhang, S., Xue, C., Yang, L., Wang, Q., Sun, X., 2010. Sediment-hosted Pb-Zn deposits in southwest Sanjiang Tethys and Kangdian area on the western margin of Yangtze Craton. Acta Geol. Sin. 84, 1428–1438.
Wang, C.M., Deng, J., Carranza, E.J.M., Lei, X.R., 2014. Nature, diversity and temporal-spatial distributions of sediment-hosted Pb-Zn deposit in China. Ore Geol. Rev. 56, 327–351.
Wei, A.Y., Xue, C.D., Xiang, K., Li, J., Liao, C., Akhter, Q.J., 2015. The ore-forming process of the Maoping Pb-Zn deposit, northeastern Yunnan, China: Constraints from cathodoluminescence (CL) petrography of hydrothermal dolomite. Ore Geol. Rev. 70, 562–577.
Wilkinson, J.J., Eyre, S.L., Boyce, A.J., 2005. Ore-forming processes in Irish-type carbonate-hosted Zn-Pb deposits: Evidence from mineralogy, chemistry, and isotopic composition of sulfides at the Lisheen mine. Econ. Geol. 100, 63–86.
Woodhead, J., Hergt, J., Meffre, S., Large, R.R., Danyushevsky, L., Gilbert, S., 2009. In situ Pb-isotope analysis of pyrite by laser ablation (multi-collector and quadrupole) ICPMS. Chem. Geol. 262, 344–354.
Xu, Y., Huang, Z., Zhu, D., Luo, T., 2014. Origin of hydrothermal deposits related to the Emeishan magmatism. Ore Geol. Rev. 63, 1–8.
Yan, Y.F., Zhong, K.H., Zhou, H.W., Chen, J., 2010. The Sichuan Ningnan silver deposits in riding the mule-ore mineral geological characteristics and shallow ore fabrics. Sichuan Nonferrous Metals 1, 1–6 (in Chinese with English abstract).
Yang, H.Y., 2009. Study on the Ore-controlling Structures in Yinchanggou-Qiluogou Pb-Zn Deposit, Ningnan, Sichuan (Master degree thesis). Chengdu University of Technology (in Chinese with English abstract).
Ye, L., Cook, N.J., Ciobanu, C.L., Liu, Y., Zhang, Q., Liu, T., Gao, W., Yang, Y., Danyushevskiy, L., 2011. Trace and minor elements in sphalerite from base metal deposits in South China: a LA-ICPMS study. Ore Geol. Rev. 39, 188–217.
Yuan, H.L., Yin, C., Liu, X., Chen, K.Y., Bao, Z.A., Zong, C.L., Dai, M.N., Lai, S.C., Wang, R., Jiang, S.Y., 2015. High precision *in-situ* Pb isotopic analysis of sulfide minerals by femtosecond laser ablation multi-collector inductively coupled plasma mass spectrometry. Sci. China Earth Sci. 58, 1713–1721.
Zartman, R.E., Doe, B.R., 1981. Plumbotectonics-the model. Tectonophysics 75, 135–162.
Zaw, K., Peters, S.G., Cromie, P., Burrett, C., Hou, Z.Q., 2007. Nature, diversity of deposit types and metallogenic relations of South China. Ore Geol. Rev. 31, 3–47.
Zhang, C., Wu, Y., Hou, L., Mao, J., 2015. Geodynamic setting of mineralization of Mississippi Valley-type deposits in world-class Sichuan-Yunnan-Guizhou Zn-Pb triangle, southwest China: implications from age-dating studies in the past decade and the Sm-Nd age of the Jinshachang deposit. J. Asian Earth Sci. 103, 103–114.
Zheng, M.H., Wang, X.C., 1991. Genesis of the Daliangzi Pb-Zn deposit in Sichuan. China. Econ. Geol. 86, 831–846.
Zheng, R.H., Gao, J.G., Nian, H.L., Jia, F.J., 2015. Rb-Sr isotopic compositions of sphalerite and its geological implications for Maozu Pb-Zn deposit, northeast Yunnan Province, China. Acta Miner. Sinica 35, 435–438 (in Chinese with English abstract).
Zhou, H.W., 2009. Yinchanggou-Qiluogou in Sichuan Ningnan County Lead-zinc Deposit Metallogenic Regularities and Metallogenic Prediction (Master degree thesis). Chengdu University of Technology (in Chinese with English abstract).
Zhou, C.X., Wei, C.S., Guo, J.Y., 2001. The source of metals in the Qilingchang Pb-Zn deposit, Northeastern Yunnan, China: Pb-Sr isotope constraints. Econ. Geol. 96, 583–598.
Zhou, M.F., Yan, D.P., Kennedy, A.K., Li, Y.Q., Ding, J., 2002. SHRIMP zircon geochronological and geochemical evidence for Neo-Proterozoic arc-related magmatism along the western margin of the Yangtze Block, South China. Earth Planet. Sci. Lett. 196, 1–67.
Zhou, J., Huang, Z., Zhou, M., Li, X., Jin, Z., 2013a. Constraints of C-O-S-Pb isotope compositions and Rb-Sr isotopic age on the origin of the Tianqiao carbonate-hosted Pb-Zn deposit, SW China. Ore Geol. Rev. 53, 77–92.
Zhou, J., Huang, Z., Yan, Z., 2013b. The origin of the Maozu carbonate-hosted Pb-Zn deposit, southwest China: constrained by C-O-S-Pb isotopic compositions and Sm-Nd isotopic age. J. Asian Earth Sci. 73, 39–47.
Zhou, J.X., Huang, Z.L., Zhou, M.F., Zhu, X.K., Muchez, P., 2014a. Zinc, sulfur and lead isotopic variations in carbonate-hosted Pb-Zn sulfide deposits, southwest China. Ore Geol. Rev. 58, 41–54.
Zhou, J.X., Huang, Z.L., Lv, Z.C., Zhu, X.K., Gao, J.G., Mirnejad, H., 2014b. Geology, isotope geochemistry and ore genesis of the Shanshulin carbonate-hosted Pb-Zn deposit, southwest China. Ore Geol. Rev. 63, 209–225.
Zhou, J.X., Bai, J.H., Huang, Z.L., Zhu, D., Yan, Z.F., Lv, Z.C., 2015. Geology, isotope geochemistry and geochronology of the Jinshachang carbonate-hosted Pb-Zn deposit, southwest China. J. Asian Earth Sci. 98, 272–284.
Zhou, J.X., Luo, K., Li, B., Huang, Z.L., Yan, Z.F., 2016. Geological and isotopic constraints on the origin of the Anle carbonate-hosted Zn-Pb deposit in northwestern Yunnan Province, SW China. Ore Geol. Rev. 74, 88–100.
Zhu, C.W., Wen, H.J., Zhang, Y.X., Fu, S.H., Fan, H.F., Cloquet, C., 2017. Cadmium isotope fractionation in the Fule Mississippi Valley-type deposit, Southwest China. Mineral. Deposita 52, 675–686.